International Journal of Microwave and Wireless Technologies

cambridge.org/mrf

Wideband low-profile aperture-coupled circularly polarized antenna based on metasurface

Qi Zheng, Chenjiang Guo and Jun Ding

School of Electronics and Information, Northwestern Polytechnical University, Xi'an, China

Research Paper

Cite this article: Zheng Q, Guo C, Ding J (2018). Wideband low-profile aperture-coupled circularly polarized antenna based on metasurface. *International Journal of Microwave and Wireless Technologies* **10**, 851–859. https://doi.org/10.1017/S1759078718000351

Received: 2 June 2017
Revised: 8 February 2018
Accepted: 12 February 2018
First published online: 22 March 2018

Key words:
Aperture-coupled antenna; circular polarization; coplanar waveguide; metasurface; wideband

Author for correspondence:
Qi Zheng, E-mail: zhq930908@mail.nwpu.edu.cn

Abstract

In this paper, a metasurface-based aperture-coupled circularly polarized (CP) antenna with wideband and high radiation gain is proposed and analyzed. The proposed antenna is comprised of coplanar waveguide coupling with 4×4 corner truncated square patches, which show compact size and low profile. The mechanism of the CP antenna is analyzed theoretically based on the mode analysis and equivalent circuit analysis. The parameters of feeding structure and truncated corner are studied and optimized to achieve wide impedance bandwidth (BW) and axial ratio (AR) BW. Finally, an overall size of 38.8 mm × 38.8 mm × 3.5 mm ($0.71\lambda_0 \times 0.71\lambda_0 \times 0.064\lambda_0$ at 5.5 GHz) CP antenna is proposed and fabricated. The simulated results demonstrate that over 41.7% impedance BW ($S_{11} < -10$ dB) of 4.55–6.95 GHz and 3 dB AR BW of 5.05–6.15 GHz (fractional BW is about 19.6%) are achieved. In addition, the antenna yielded a broadside CP radiation with a high gain average about 7.5 dBic. Experimental results are in good agreement with the simulated ones.

Introduction

Over the past few decades, circularly polarized (CP) antenna has attracted a lot of interests due to its wide applications in satellite communication system, radio frequency identification (RFID), wireless sensors, and so on [1]. Generally speaking, CP antenna mainly includes two categories, single-feed and dual/multi-feed. The latter one always requires power divider or complicated feeding network, which is not beneficial to design and manufacture. Hence, several attentions have been focused on single-feed CP antenna, which can be easily miniaturized and integrated. Many technologies have been applied to achieve CP radiation, such as varies shaped patch [2], short pins [3], and cross slotted patch [4]. However, one drawback of the former one is its narrow impedance matching bandwidth (BW) and axial ratio (AR) BW due to high value of quality factor Q.

In order to broaden its BW, several techniques have been proposed, such as thick air substrate [5], slot loading [6], stacked patches [7]. However, these designs are always bulky and low radiation efficiency, which are not practical to achieve compact size and high efficiency. To overcome these drawbacks, many novel types of antenna are reported, especially metamaterial-based or metasurface-based structures. In [8], a partially reflective surface (PRS) and artificial impedance surface-based resonant cavity structure was applied to improve radiation gain of CP antenna. Besides, metamaterial-based CP antenna with linearly polarized (LP) wave has attracted much attention [9–11], which can simplify the design procedure of CP radiator source. For example, metamaterial-based PRSs have been used to design high gain CP Fabry–Perot cavity antenna [9, 10]. However, most of these designs require a distance between radiator and PRS to satisfy cavity resonance condition. Therefore, some CP antennas with metamaterials under the radiator have been proposed [12, 13]. Yang *et al.* [13] proposed a low-profile CP antenna with a height of $0.04\,\lambda_0$ using a polarization rotating reflective surface based on artificial magnetic conductor, while it is still a challenging problem to obtain wider BW.

Recently, another method by integrating metasurface into a traditional LP aperture antenna was proposed to enhance BW and reduce volume [14–20]. Liu *et al.* [14, 15] proposed low-profile broadband mushroom-based and grid slotted metamaterial-based planar antennas by exciting two modes simultaneously. Then, some designs of feeding structure are used to achieve CP radiation based on the two designs [16]. In [16], a low-profile grid-slotted CP patch antenna achieves wide impedance BW and 3 dB AR BW using Z-shaped slotted ground. Another method to obtain circular polarization is using CP metamaterial units array, such as corner truncated patches [17, 18, 21]. Different polarization states and radiation patterns are realized owning to some perturbation segments of the truncated corner. However, the wide AR BW of the design is still a challenge. Specifically, with the development of satellite and wireless communication systems, the demands on the antenna are required higher and higher. The

© Cambridge University Press and the European Microwave Association 2018

CAMBRIDGE UNIVERSITY PRESS

antenna design to satisfy these requirements, such as wide operating BW, compact volume and miniaturized size, is a valuable research.

In this paper, a low-profile slot antenna based on metasurface for C-band satellite communication is proposed and studied. The period size of the metasurface is 0.18 λ_0 at center frequency, which shows advantages for miniaturized design. The proposed antenna consists of 4 × 4 unit cells printed on top substrate without air gap, which indicate its superiority for reducing total volume. Besides, compared with published literatures, the mechanism of the metasurface-based antenna is detailed and analyzed based on mode analysis, surface current distributions, and equivalent circuit transmission mode, respectively. The measurements are also given in detail. Further study of parameters reveals key impacts of the antenna and provides design guidelines. Full-wave simulations using commercial software ANSYS HFSS and experimental measurements are carried out to verify the previous analysis and radiation performances of the antenna.

Design and analysis of antenna

Design and full-wave simulation

The proposed antenna geometry is shown in Fig. 1, which consists of three layers. The two layers of dielectric substrates are Arlon AD350A [22] (a dielectric constant $\varepsilon_r = 3.5$, and a loss tangent $\tan\delta = 0.003$) with thickness of $h_1 = 0.5$ mm and $h_2 = 3$ mm, respectively. There is no air gap between two substrates, so the volume of the antenna is reduced. The top metasurface with 4 × 4 corner truncated square patches is printed on upper substrate. The lower substrate is sandwiched between middle slotted ground plane and bottom SMA connector and feeding line, which works as a conventional slot antenna. Optimizing parameters of the feeding structure and the truncated corner using commercial software ANSYS HFSS versus 13.0, wide impedance BW and CP BW is realized. The parameters are optimized as follows: $p = 9.7$ mm, $a = 9.2$ mm, $b = 3$ mm, $l_g = 38.8$ mm, $l_s = 27$ mm, $w_s = 2$ mm, $l_f = 26.4$ mm, $w_f = 1.2$ mm, $l_g = 14$ mm, $w_g = 6$ mm, $g_f = 0.7$ mm.

To illustrate why CP radiation can be achieved by the proposed metasurface-based antenna, we make comparisons between two slot antennas, as presented in Fig. 2. Ant I is a traditional slot antenna and consists of a ground plane with air slot, feeding line, and two dielectric substrates, as shown in Fig. 2(a). Ant II is a square metasurface-based slot antenna, which is comprised of 4 × 4 square patches printed on upper substrate and the other components are the same as Ant I, as shown in Fig. 2(b). It should be noticed that the parameters of the three antennas are chosen as the same for a fair comparison, such as feeding structure, thickness of two substrates, and period of metasurface and so on.

Figure 3 presents simulated S_{11} and gain of three antennas. AR of the proposed antenna is given in Fig. 3(b). It is known that Ant I and Ant II are LP antennas and the AR are not depicted for simplicity. For Ant I, there is a resonance at 6.40 GHz with $S_{11} = -8.80$ dB. For Ant II, there are two resonance frequencies occurring at 4.90 GHz ($S_{11} = -27.80$ dB) and 6.20 GHz ($S_{11} = -23.20$ dB). It can be seen that the impedance BW is changed and the gain is improved by metasurface. The main reason is that the metasurface-based antenna exited two adjacent resonant modes (TM_{10} mode and antiphase TM_{20} mode) [15]. The polarization state is also not affected by square metasurface. Hence, the proposed antenna

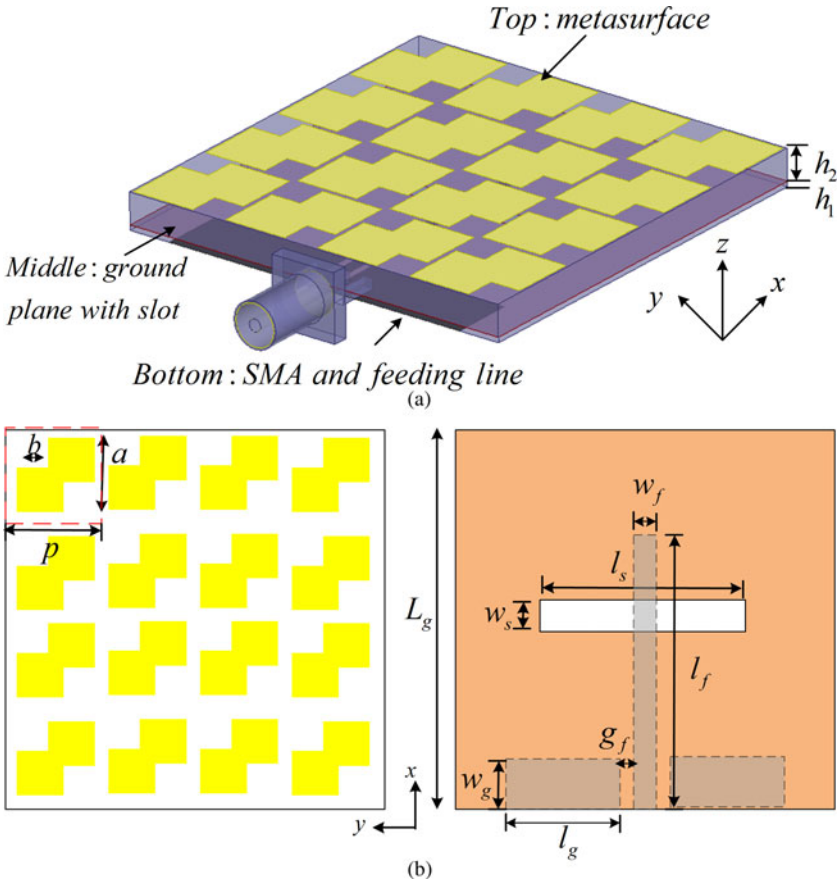


Fig. 1. (a) Schematic view. (b) Front view of top, middle, and bottom structures of the proposed antenna.

https://doi.org/10.1017/S1759078718000351 Published online by Cambridge University Press

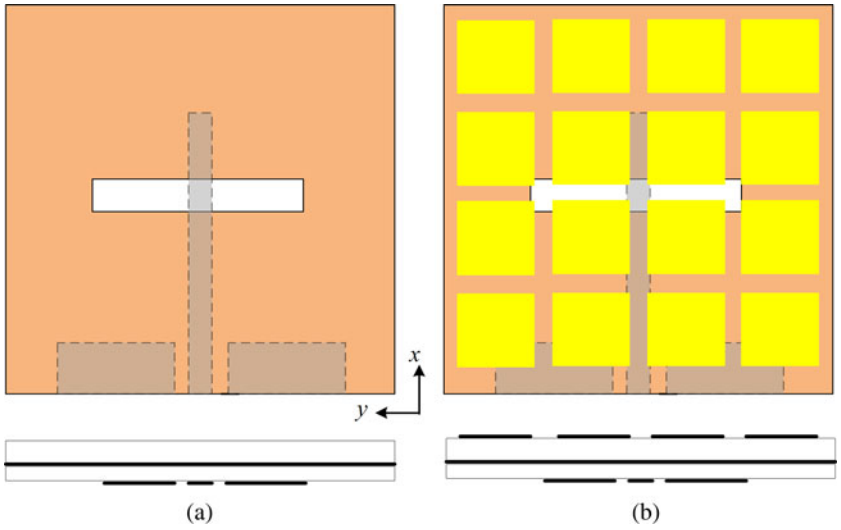


Fig. 2. Schematic view of (a) Ant I and (b) Ant II.

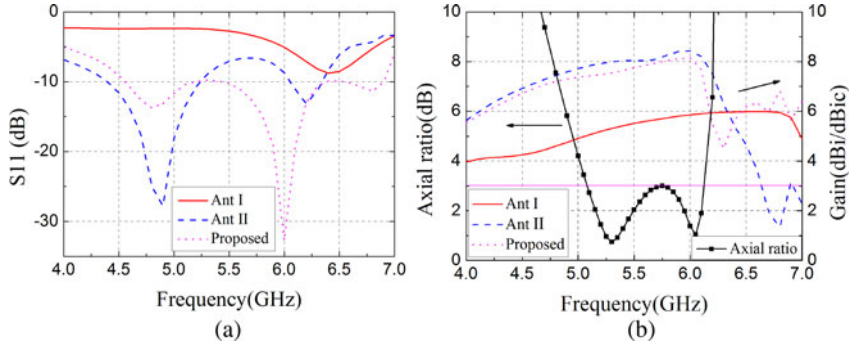


Fig. 3. Simulated results of (a) S_{11} and (b) AR and gain.

is designed by adjusting the size of the truncated corner of the square patches to obtain CP radiation. The simulated results demonstrate that about 41.7% impedance BW (4.55–6.95 GHz) and 19.6% 3 dB AR BW (5.05–6.15 GHz) are realized. The simulated efficiency is over 95% in the entire operation band. Furthermore, a broadside gain of 7.40–8.15 dBic is achieved at the same time.

Besides, similar to the analysis in [23], numerical studies are carried out to further explain radiation performance of the antenna. As the radiated electric fields in the far-field boresight (+z) direction can be decomposed into two orthogonal components ($\vec{E}_x$ and $\vec{E}_y$), the phase, phase difference, and magnitude ratio $|\vec{E}_x|/|\vec{E}_y|$ are investigated to examine circular polarization. Figure 4(a) depicts the phase and phase difference between the two orthogonal components, which are named as φ_x, φ_y and $\varphi_x - \varphi_y$, respectively. It can be seen that the phase difference is roughly − 90° in the frequency range of 5.0–6.1 GHz. The magnitude ratio is also between ± 3 dB in the band, as presented in Fig. 4(b).

Mode analysis

To study the physical principle at two resonance frequencies in the AR BW of 5.30 GHz (AR = 0.75 dB) and 6.05 GHz (AR = 1.00 dB) given in Fig. 3(b), the electric field distributions are presented in Fig. 5. It is validated that the two resonance modes are TM_{10} mode and antiphase TM_{20} mode, which are the same with Ant II. The small frequency shift is mainly due to the size change of the patches. Figures 6 and 7 present surface current distributions on the metasurface vary with phase at two resonance modes, respectively. As can be seen from the figures, the domain

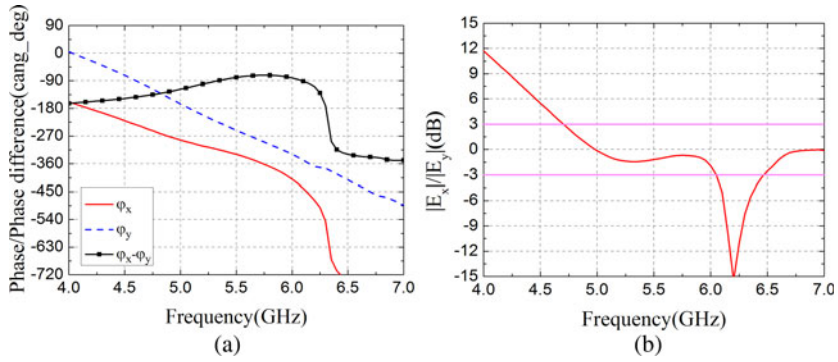


Fig. 4. Simulated results of (a) phase, phase difference, and (b) magnitude ratio between the radiated electric fields of two orthogonal components ($\vec{E}_x$ and $\vec{E}_y$).

https://doi.org/10.1017/S1759078718000351 Published online by Cambridge University Press

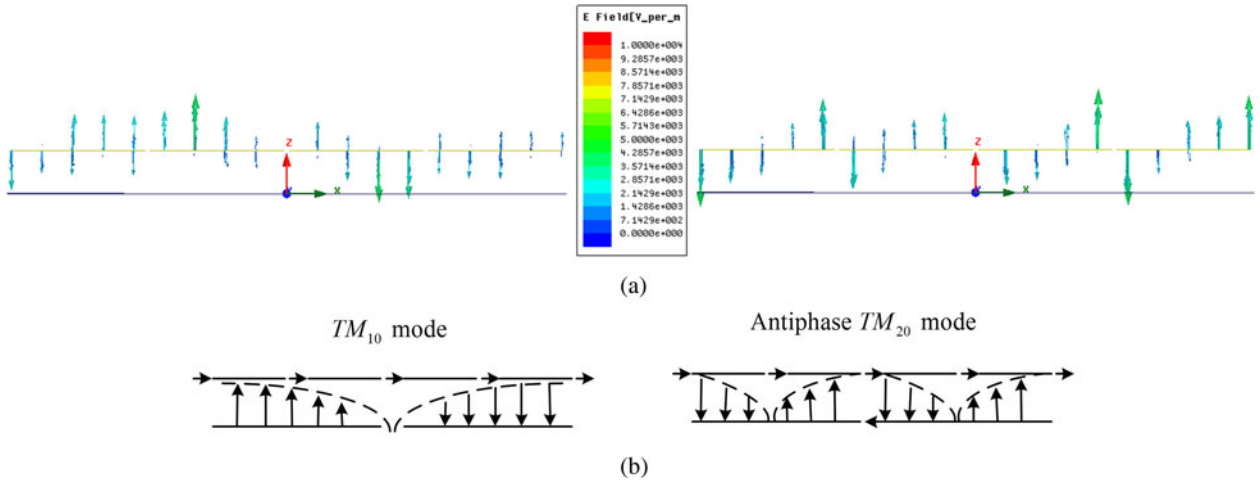


Fig. 5. (a) Electric field distributions and (b) sketch diagram at two resonance modes.

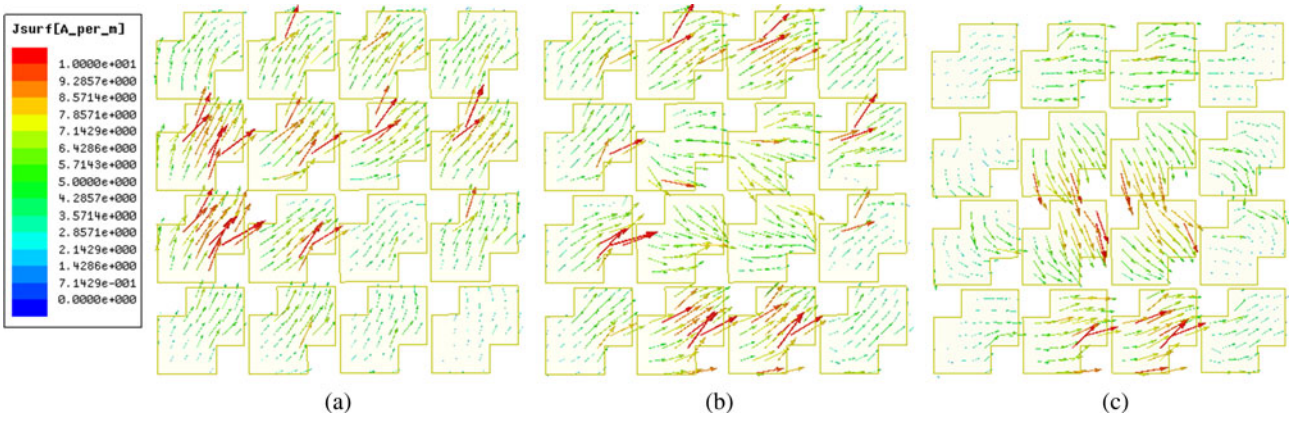


Fig. 6. Surface current distributions at 5.30 GHz (a) $wt = 0°$; (b) $wt = 45°$; (c) $wt = 90°$.

current direction changes in clockwise order with time phase (wt) varies from 0 to 90° (step 45°), which means a LHCP is realized.

Equivalent circuit analysis

To further explain the operating mechanism of CP radiation, we extract a new unit cell of the metasurface and its equivalent circuit [17, 21] seen by diagonal direction is displayed in Fig. 8. The LP wave excited from the microstrip slot antenna (direction of $\vec{E}$ is along x-axis for the proposed antenna) can be decomposed as two orthogonal components along diagonal directions ($\vec{E}_1$ and $\vec{E}_2$). Then the impedances satisfy the following equations:

$$Z_1 = R_1 + j\omega L_1 + 1/j\omega C_1, \quad (1)$$

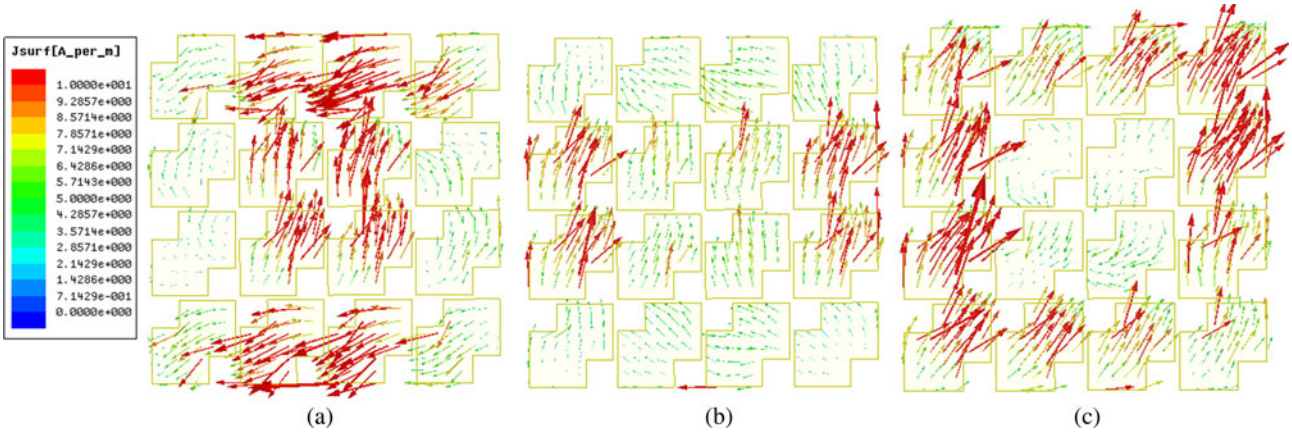


Fig. 7. Surface current distributions at 5.05 GHz (a) $wt = 0°$; (b) $wt = 45°$; (c) $wt = 90°$.

https://doi.org/10.1017/S1759078718000351 Published online by Cambridge University Press

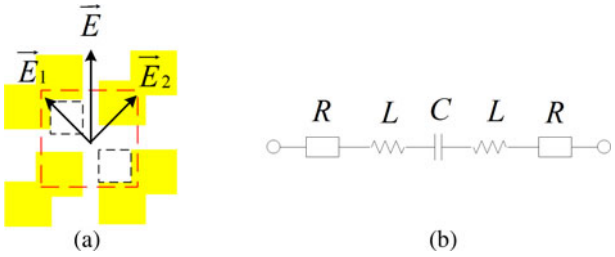


Fig. 8. (a) New unit cell. (b) Equivalent circuit model.

$$Z_2 = R_2 + j\omega L_2 + 1/j\omega C_2, \tag{2}$$

where R_i, L_i, and C_i ($i = 1, 2$) are the resistance, inductance, and capacitance of two adjacent new unit cells in two diagonal directions. The value of Z_1 and Z_2 changes with the variation of the truncated corner, then the electric fields will be changed. Hence, we can alter radiation performance by adjusting the parameters of truncated corner. To realize CP radiation, the impedance along two diagonal directions needs to satisfy

$$|Z_1| = |Z_2|, \tag{3}$$

$$\angle Z_1 - \angle Z_2 = \pm 90^0. \tag{4}$$

Hence, circular polarization can be realized.

Study of the parameters

As mentioned before, the impedance BW and AR BW are dependent on the feeding structure and metasurface parameters. Therefore, the influence of feeding structure on the performances of the proposed antenna is studied in the first part. As the slot length l_s and thickness h_2 of the upper substrate play important roles in the design, the antenna performances under these variations are focused. Then the effects of several key parameters of the metasurface are investigated in the second part, including the variation of period size p, length a, and truncated corner size b. It is noted that the influence of the specific parameter is examined with the other parameters that are fixed.

Effect of the feeding structure

The S_{11}, AR, and gain varies with different slot length l_s are presented in Fig. 9. It is known that the slot length has an important impact on resonant modes. Figure 9(a) depicts that the impedance band shifts to lower frequency with the increases of slot length, which is expected as the increases of resonant path. Simultaneously, two resonant modes shift to lower frequencies, while the radiation gain has few changes, as shown in Fig. 9(b).

Figure 10(a) gives the influence of different thickness h_2 of upper substrate on S_{11}. The impedance band shifts to lower one as the thickness increases. From Fig. 10(b), the increasing of thickness results in the decreases of AR band with gain curves shifting to lower frequencies. The phenomenon is due to the increases of the total equivalent dielectric constant.

Effect of the metasurface

Figure 11 shows S_{11}, AR, and gain of the antenna with increasing of period size p. As given in Fig. 11(a), with the increases of period size, the impedance band narrows, specifically the lower frequencies, is shifted to higher frequencies while the higher part is almost unchanged. Besides, from Fig. 11(b), the two resonant modes and gain values shift to higher ones when the period size increases from 9.5–9.7 mm.

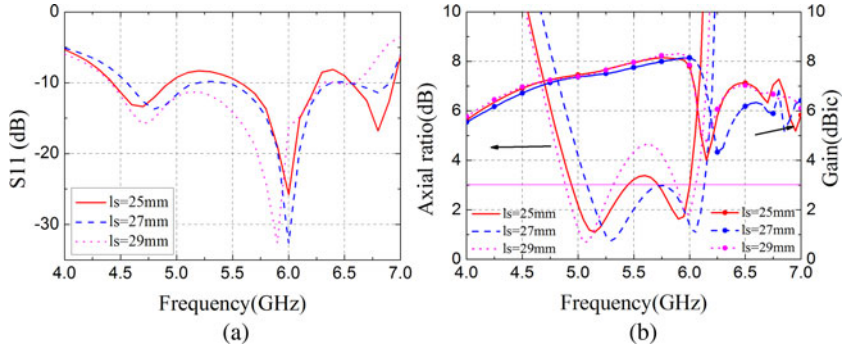


Fig. 9. (a) S_{11}, (b) AR and gain at different l_s.

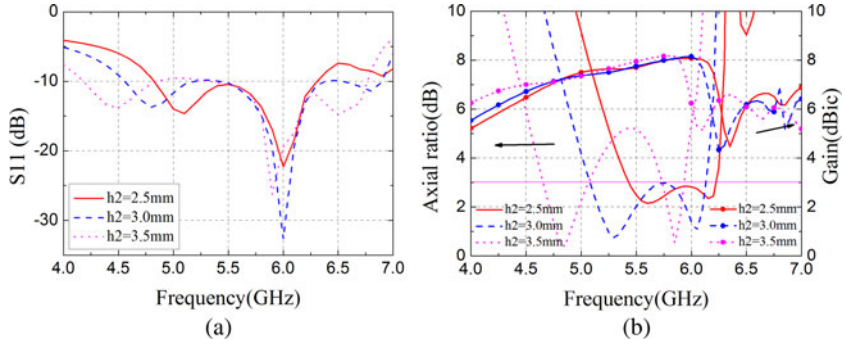


Fig. 10. (a) S_{11}, (b) AR and gain at different h_2.

https://doi.org/10.1017/S1759078718000351 Published online by Cambridge University Press

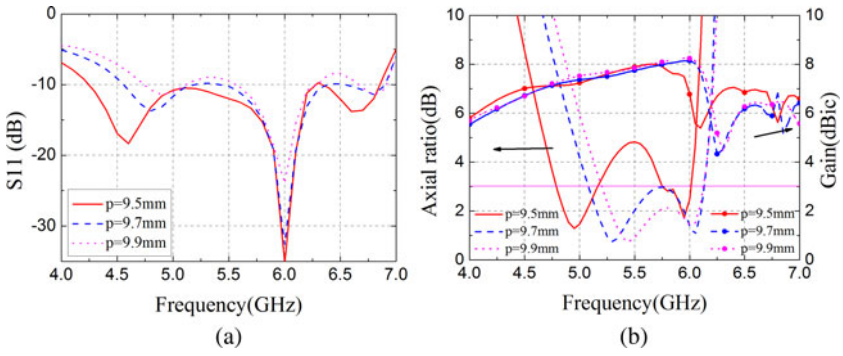


Fig. 11. (a) S_{11}, (b) AR and gain at different *p*.

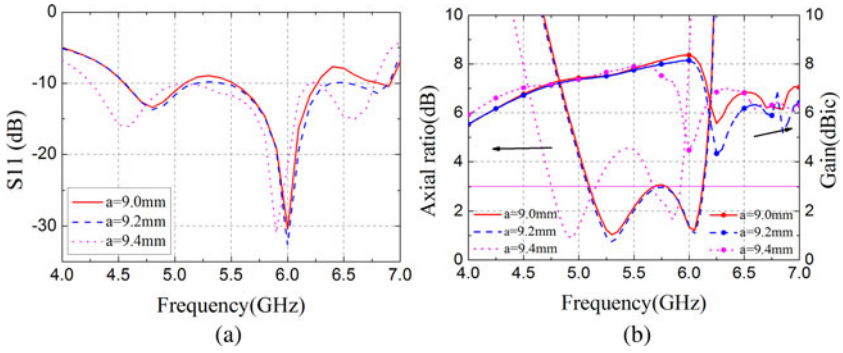


Fig. 12. (a) S_{11}, (b) AR and gain at different *a*.

As displayed in Figs 12(a) and 12(b), the length *a* of the metasurface has a significant influence on the impedance matching and AR BW. From Fig. 12(a), the impedance matching BW is expanded with the length *a*, which increases from 9.0–9.4 mm. It can be seen from Fig. 12(b) that the two resonant modes shift to lower frequencies with the increases of the length *a*, which is attributed to increases of equivalent resonant length. The curves of gain also shift to lower frequencies with increases of metasurface length.

The effects of the truncated corner size *b* on the antenna performances are given in Figs 13(a) and 13(b), respectively. Different from the influence of metasurface length *a*, the variation of truncated corner size *b* has much more impact on the impedance matching but less influence on the impedance band shift. Figure 13(a) shows that the impedance matches better with the BW, which is nearly unchanged when the size *b* increases from 2.5–3.5 mm. Figure 13(b) indicates that the AR BW varies with the increases of the truncated corner size *b* and split into two resonant frequencies gradually. The curves of gain shift to higher frequencies with the increases of the size *b*.

In a word, the antenna performances can be tuned by the mentioned parameters. The parameters optimization mainly includes two steps: (1) design of feeding structure and (2) optimization of metasurface. Then the good impedance matching and AR BW are realized.

Fabrication and measurements

In order to verify the simulations and analysis, an oversize of 38.8 mm × 38.8 mm × 3.5 mm antenna was fabricated and measured. Top and bottom views of the sample are shown in Figs 14(a) and 14(b), respectively. The antenna is fed with 50 Ω SMA connector and the reflection coefficient S11 is measured by a vector network analyzer (Agilent PNA Series Network Analyzer E8363B). The measurement can be divided into two steps. First step is the calibration of the vector network analyzer by using a calibration kit (N4692A) before the measurement. Second step is the measurement of S_{11}. The reflection coefficient of the antenna was obtained.

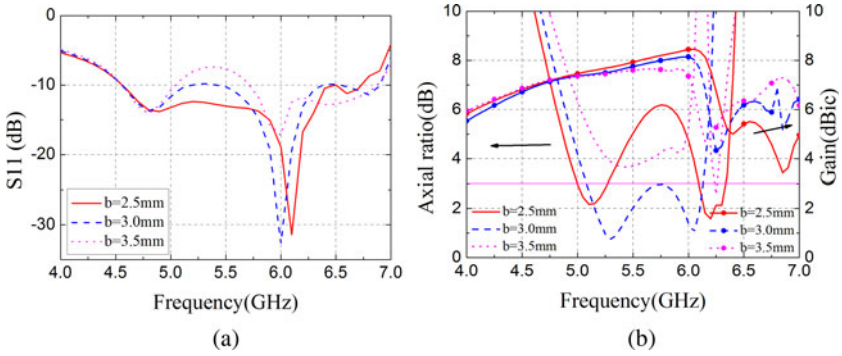


Fig. 13. (a) S_{11}, (b) AR and gain at different *b*.

https://doi.org/10.1017/S1759078718000351 Published online by Cambridge University Press

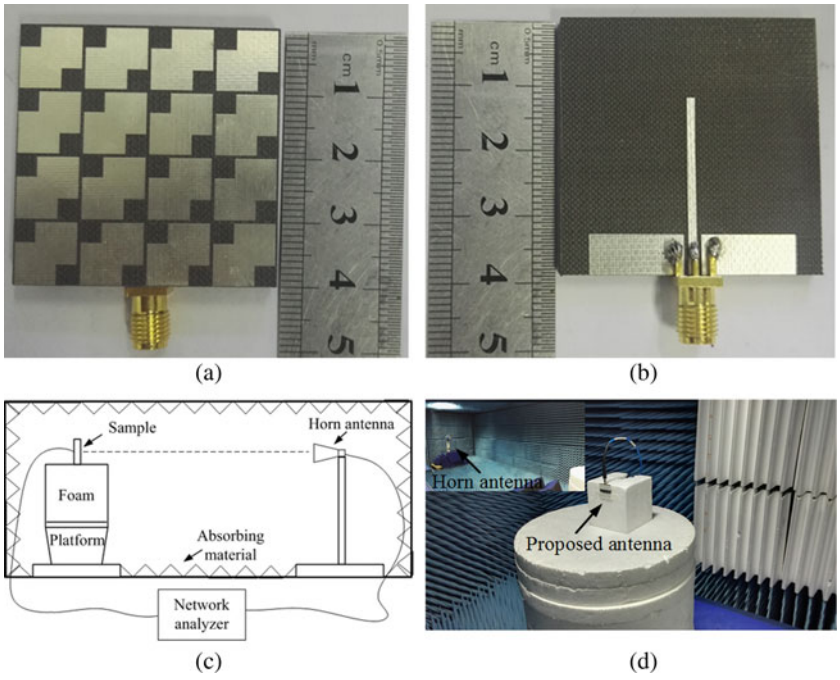


Fig. 14. (a) Top view and (b) bottom view of the antenna. (c) Schematic view of the antenna measurement setup and (d) testing in an anechoic chamber.

In practical application, we pay more attention on its AR BW, radiation patterns, and gain of CP antenna. Thus, the proposed antenna was tested by Agilent PNA Series Network Analyzer MS4644A and in the anechoic chamber (an overall size of length × width × height is 5 m × 4 m × 3 m). The schematic view of the measurement setup and practical testing are given in Figs 14(c) and 14(d), respectively. As shown in Fig. 14(c), the distance between the standard LP horn antenna and the sample is over 4 m to obtain far-field situation. Far-field can be satisfied according to the distance requirement of over $2D^2/\lambda$, where D is the largest antenna diameter [24] (physical dimensions of 38.8 mm × 38.8 mm in the case) and λ is the wavelength (42.86 mm at maximum working frequency 7.0 GHz).

Figure 14(d) displays measurement photograph of the radiation patterns and radiation gain. Considering operating BW of the proposed antenna, the standard gain antenna BJ-48 was chosen as a reference antenna, which could cover the BW of 3.94–5.99 GHz. The gain measurement includes three steps. First, the standard gain antenna was placed on the platform as a sample and its gain was measured. Second, the measured gain values were compared with standard gain curve provided by the manufacturer, such that the relative values between the actual gain values and the measured ones in the anechoic chamber of the antenna can be obtained. Third, gain of the proposed antenna was measured. Then the measured results added the relative gain values of the measurement, which are the actual radiation gain of the proposed antenna. It is noted that the results should be compared with the standard gain antenna at the same situation. Thus, we carried on the measurement of the proposed antenna after the measurement of the reference antenna immediately.

To obtain AR of the proposed antenna, a LP horn antenna was employed to measure electric fields along the orientations of the radiation far-field in boresight direction, which are named as E-ϕ ($\vec{E}_\phi$) and E-θ ($\vec{E}_\theta$), respectively. The amplitudes and phases of the two components ($\vec{E}_\phi$ and $\vec{E}_\theta$) were measured, then right-handed electric field $\vec{E}_R$, the left-handed electric field $\vec{E}_L$ are calculated according to the expressions $\vec{E}_R = (\vec{E}_\theta + j\vec{E}_\phi)/\sqrt{2}$, $\vec{E}_L = (\vec{E}_\theta - j\vec{E}_\phi)/\sqrt{2}$. Hence, the AR can be obtained according to the equation:

$$AR = \left|\left(\left|\vec{E}_R\right| + \left|\vec{E}_L\right|\right)/\left(\left|\vec{E}_R\right| - \left|\vec{E}_L\right|\right)\right|.$$

As can be seen from Fig. 15(a), measured impedance matching BW ($S_{11} < -10$ dB) is 4.40–6.60 GHz (fractional BW of 40%),

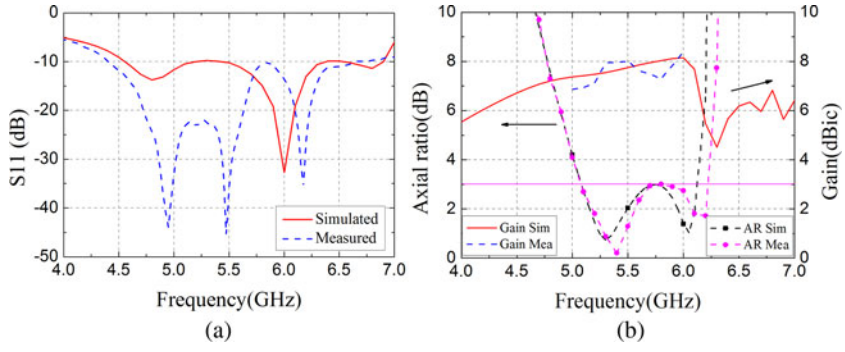


Fig. 15. (a) Simulated and measured results of S_{11}. (b) AR and gain.

https://doi.org/10.1017/S1759078718000351 Published online by Cambridge University Press

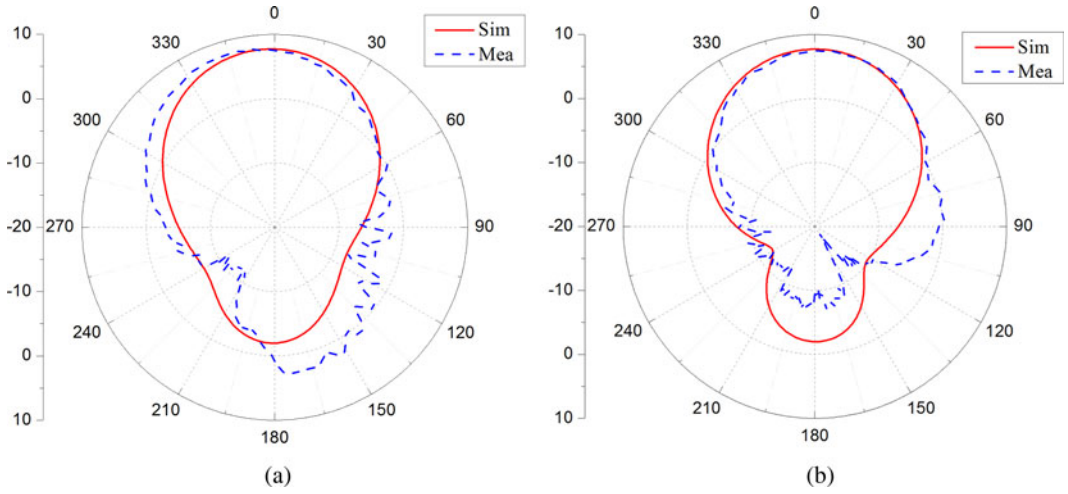


Fig. 16. Radiation patterns of (a) *xoz*-plane and (b) *yoz*-plane at 5.30 GHz.

Table 1. Measured results comparisons of recently reported wideband low-profile CP antenna

Works	f_0 (GHz)	ε_r	$S_{11} < -10$ dB BW (%)	3 dB AR BW (%)	Size (λ_0^3)
Ref. [11]	2.45	3.48	25.7	8.0	0.98 × 0.98 × 0.08
Ref. [13]	5	2.2	16.8	18	0.86 × 0.86 × 0.04
Ref. [19]	5.25	4.4	33.7	16.5	0.60 × 0.49 × 0.07
Ref. [20]	5.7	4.5	21	13.4	1.43 × 1.43 × 0.08
Ref. [23]	5.6	3.6	32	20	0.75 × 0.73 × 0.09
This work	5. 5	3.5	40	21	0.71 × 0.71 × 0.064

whereas the simulated one is 4.55–6.95 GHz (41.7% BW). Measured values of AR and gain are depicted in Fig. 15(b). It is shown that about 21% 3 dB AR BW can be achieved in the frequency range of 5.05–6.25 GHz, whereas the simulated one is 5.05–6.15 GHz (fractional BW is about 19.6%). The radiation gain was obtained compared with the standard gain antenna (3.94–5.99 GHz), so that values from 5.00 to 6.00 GHz are given to verify simulations. It is obvious that the curve of measurements has similar tendency with the simulated one and the average gain is about 7.5 dBic. Small frequency shift and deviations compared with simulated ones are acceptable considering fabrication errors and measurement errors. Radiation patterns of *xoz*-plane and *yoz*-plane at first resonance mode are given as an example to study radiation performance of the antenna, as shown in Fig. 16. The measured and simulated radiation patterns show good agreement in a broadside radiation. The deviations at back side are mainly caused by measurement errors, such as the influence of testing coaxial cable. Radiation patterns at other frequencies have similar features within the CP operating band.

Measured results of recently reported metasurface-based CP antenna and our work are concluded in Table 1. The comparisons show that the proposed low-profile antenna owns properties of wide impedance matching BW, wide operating AR BW, and high gain. Besides, the coplanar waveguide feeding structure generates compact size and miniaturization.

Conclusion

In this work, we proposed a wideband CP aperture-coupled antenna based on the metasurface due to the polarization conversion of the patches. The integrated metasurface patches and coplanar waveguide feed structure ensures its compactness and low profile. The theoretical analysis and parametric studies serve as a guideline for wideband design. Simulated results demonstrate about 41.7% impedance matching BW ($S_{11} < -10$ dB) of 4.55–6.95 GHz and 19.6% AR BW of 5.05–6.15 GHz. Besides, an antenna sample was fabricated and measured. The measured results and the simulated ones are in good agreement. The CP antenna is low profile, wideband, and high gain, which shows a potential application for C-band satellite and wireless communication system.

Acknowledgement. The authors thank the reviewers and the editors for their valuable comments and warm work earnestly.

References

[1] **Gao S, Luo Q and Zhu F** (2014) *Circularly polarized antennas*. Chichester, UK: John Wiley & Sons.

[2] **Chen HM and Wong KL** (1999) On the circular polarization operation of annular-ring microstrip antennas. *IEEE Transactions on Antennas and Propagation* **47**, 1289–1292.

[3] **Wong H, So KK, Ng KB, Lug KM, Chan CH and Xue Q** (2010) Virtually shorted patch antenna for circular polarization. *IEEE Antennas and Wireless Propagation Letters* **9**, 1213–1216.

[4] **Chen ZN and Qing X** (2012) A compact circularly polarized cross-shaped slotted microstrip antenna. *IEEE Transactions on Antennas and Propagation* **60**, 1584–1588.

[5] **Yang SLS, Lee KF, Kishk AA and Luk KM** (2008) Design and study of wideband single feed circularly polarized microstrip antennas. *Progress in Electromagnetics Research* **80**, 45–61.

[6] **Su CW, Chang FS and Wong KL** (2003) Broadband circularly polarized inverted-L patch antenna. *Microwave and Optical Technology Letters* **38**, 134–136.

[7] **Oraizi H and Pazoki R** (2013) Wideband circularly polarized aperture-fed rotated stacked patch antenna. *IEEE Transactions on Antennas and Propagation* **61**, 1048–1054.

[8] **Zhao G, Jiao YC, Zhang F and Yang X** (2010) High gain circularly polarized antenna using sub-wavelength resonant cavity. *Journal of Electromagnetic Waves and Applications* **24**, 33–40.

https://doi.org/10.1017/S1759078718000351 Published online by Cambridge University Press

[9] **Orr R, Goussetis G and Fusco V** (2014) Design method for circularly polarized Fabry–Perot cavity antennas. *IEEE Transactions on Antennas and Propagation* **62**, 19–26.
[10] **Liu ZG and Wei-Bing LU** (2017) Low-profile design of broadband high gain circularly polarized Fabry-Perot resonator antenna and its array with linearly polarized feed. IEEE Access.
[11] **Zhu HL, Cheung SW, Chung KL and Yuk TI** (2013) Linear-to-circular polarization conversion using metasurface. *IEEE Transactions on Antennas and Propagation* **61**, 4615–4623.
[12] **Yang F and Rahmat-Samii Y** (2005) A low profile single dipole antenna radiating circularly polarized waves. *IEEE Transactions on Antennas and Propagation* **53**, 3083–3086.
[13] **Yang W, Tam KW, Choi WW, Che W and Hui HT** (2014) Novel polarization rotation technique based on an artificial magnetic conductor and its application in a low-profile circular polarization antenna. *IEEE Transactions on Antennas and Propagation* **62**, 6206–6216.
[14] **Liu W, Chen ZN and Qing X** (2014) Metamaterial-based low-profile broadband mushroom antenna. *IEEE Transactions on Antennas and Propagation* **62**, 1165–1172.
[15] **Liu W, Chen ZN and Qing X** (2015) Metamaterial-based low-profile broadband aperture-coupled grid-slotted patch antenna. *IEEE Transactions on Antennas and Propagation* **63**, 3325–3329.
[16] **Lin FH, Chen ZN, Liu W and Chen ZN** (2015) A metamaterial-based broadband circularly polarized aperture-fed grid-slotted patch antenna. Antennas and Propagation (APCAP), 2015 IEEE 4th Asia–Pacific Conference; Kuta, Indonesia, 353–354.
[17] **Zhu HL, Cheung SW, Liu XH and Yuk TI** (2014) Design of polarization reconfigurable antenna using metasurface. *IEEE Transactions on Antennas and Propagation* **62**, 2891–2898.
[18] **Sali NM and Paul B** (2015) A 2.4 GHz polarization reconfigurable metasurface antenna. Advances in Computing and Communications (ICACC), 2015 Fifth International Conference on. IEEE; Kochi, India, 254–257.
[19] **Wu Z, Li L, Li Y and Chen X** (2016) Metasurface superstrate antenna with wideband circular polarization for satellite communication application. *IEEE Antennas and Wireless Propagation Letters* **15**, 374–377.
[20] **Jia Y, Liu Y and Gong S** (2016) Wideband high-gain circularly polarized planar antenna based on polarization rotator. Electromagnetics in Advanced Applications (ICEAA), 2016 International Conference on. IEEE; Cairns, Australia, 416–419.
[21] **Huang Y, Yang L, Li J, Wang Y and Wen G** (2016) Polarization conversion of metasurface for the application of wide band low-profile circular polarization slot antenna. *Applied Physics Letters* **109**, 054101.
[22] **RF Globalnet for RF components, RF test and measurement, ICs, RF modules [Online].** Available at https://www.rfglobalnet.com.
[23] **Altintas O, Unal E, Akgol O, Karaaslan M, Karadag F and Sabah C** (2017) Design of a wide band metasurface as a linear to circular polarization converter. *Modern Physics Letters B* **31**, 1750274.
[24] **Kraus JD and Marhefka RJ** (2002) *Antennas for all applications*, 3rd edn., New York: McGraw Hill.



Qi Zheng was born in Anhui Province, China, in 1993. He received the B.Sc. in Mathematics and Applied Mathematics from the School of Science, Northwestern Polytechnical University (NPU), 2014. Then, he received the M.Sc. in Electromagnetic Field and Microwave Technology from the School of Electronic and Information, NPU, 2016. Now, he is pursuing the Ph.D. degree in Electronic Science and Technology from the School of Electronic and Information, NPU. His research interests include design of reflect array, electromagnetic metamaterials, and RCS reduction. E-mail: zhq930908@mail.nwpu.edu.cn



Chenjiang Guo was born in Shaanxi Province, China, in 1963. CIE Senior Member, Antenna Society Committee Member. He received the M.Sc., B.Sc, and Ph.D. from the School of Electronics and Information, Northwestern Polytechnical University in Xi'an city, China, in 1984, 1987, and 2007, respectively. He is a professor in the School of Electronics and Information NWPU. He has published more than 140 research papers. His research interests include EMI/EMC, the antenna theory and design, and the microwave circuit design. E-mail: cjguo@nwpu.edu.cn



Jun Ding was born in Shaanxi Province, China, in 1964. She received the M.Sc., B.Sc., and Ph.D. from the School of Electronics and Information, Northwestern Polytechnical University in Xi'an city, China, in 1986, 1989, and 2005, respectively. She is a professor in the School of Electronics and Information NWPU. She has published more than 100 research papers. Her research interests include electromagnetic metamaterials, the antenna theory and design, and the microwave circuit design. E-mail: dingjun@nwpu.edu.cn

https://doi.org/10.1017/S1759078718000351 Published online by Cambridge University Press